

Charmonium potential from full lattice QCD

Taichi Kawanai^{1,2,3*} and Shoichi Sasaki^{1†}

¹*Department of Physics, The University of Tokyo, Hongo 7-3-1, Tokyo 113-0033, Japan*

²*RIKEN-BNL Research Center, Brookhaven National Laboratory Upton, NY 11973-5000, USA and*

³*Department of Physics, Brookhaven National Laboratory Upton, NY 11973-5000, USA*

(Dated: October 25, 2018)

We present both spin-independent and -dependent parts of a central interquark potential for charmonium states, which is calculated in 2+1 flavor dynamical lattice QCD using the PACS-CS gauge configurations with a lattice cutoff of $a^{-1} \approx 2.2$ GeV. Our simulations are performed with a relativistic heavy-quark action for the charm quark at the lightest pion mass, $M_\pi = 156(7)$ MeV, in a spatial volume of $(3 \text{ fm})^3$. We observe that the spin-independent charmonium potential obtained from lattice QCD with almost physical quark masses is quite similar to the Cornell potential used in nonrelativistic potential models. The spin-spin potential, which is calculated in full lattice QCD for the first time, properly exhibits a finite-range repulsive interaction. Its r -dependence is different from the Fermi-Breit type potential, which is widely adopted in quark potential models.

Recently, many of the newly discovered charmonium-like mesons have been announced by B -factories at KEK and SLAC, which are primarily devoted to the physics of CP violation. Such states named as “ XYZ ” mesons could not be simply explained by a constituent quark description in quark potential models [1]. Thus, the charmoniumlike XYZ mesons are expected to be good candidates for nonstandard quarkonium mesons such as hadronic molecular states, diquark-antidiquark bound states (tetraquark states) or hybrid mesons [2]. However, it seems to be still too early to judge whether we may discard the constituent quark description for such higher-mass charmonium states.

The interquark potential in quark potential models is based on the phenomenology of confining quark interactions: the so-called Cornell potential [3] together with spin-spin, tensor and spin-orbit terms appeared as leading spin-dependent corrections in powers of the inverse of the heavy-quark mass m_Q [4, 5]. Although the Cornell potential was qualitatively justified by the static heavy-quark potential obtained from Wilson loops in lattice QCD [6], the functional forms of the spin-dependent terms in potential models are basically determined by perturbative one-gluon exchange as the Fermi-Breit type potential [4]. Thus, properties of higher-mass charmonium states predicated in potential models may suffer from large uncertainties, since the phenomenological spin-dependent potentials would have validity only at short distances and also in the vicinity of the heavy-quark mass limit.

In this sense, the reliable interquark potential directly derived from first principles QCD is desired at the charm quark mass. Indeed, the static potential between infinitely heavy-quark and antiquark, which is obtained from Wilson loops, have been precisely calculated in lattice QCD simulations [6]. The relativistic corrections to the static potential are classified in powers of $1/m_Q$ within a framework called potential nonrelativistic QCD [7]. The leading and next-to-leading order cor-

rections have been successfully calculated in quenched lattice QCD with high accuracy by using multilevel algorithm [8]. However, it is rather difficult to calculate the proper *charmonium* potential in lattice QCD within the Wilson loop formalism. It is obvious that the inverse of the charm quark mass is far outside the validity region of the $1/m_Q$ expansion. Indeed, a spin-spin potential determined at $\mathcal{O}(1/m_Q^2)$ [8], which exhibit an attractive interaction for the higher spin states, seems to yield wrong mass ordering among hyperfine multiplets. In addition, practically, the multilevel algorithm employed in Ref. [8] is not easy to be implemented in dynamical lattice QCD simulations.

Under these circumstances, in our previous work [9], we have proposed a novel approach, where the interquark potential at finite quark mass can be accurately determined from the equal-time and Coulomb gauge Bethe-Salpeter (BS) amplitude through an effective Schrödinger equation (See also Ref. [10]). The BS amplitude method is originally applied for the hadron-hadron interaction [11]. As demonstrated in Ref. [9], the spin-independent part of an interquark potential calculated in the new method smoothly approaches the static potential given by Wilson loops in the infinitely heavy-quark limit. The new approach enables us to determine both spin-independent and spin-dependent interquark potentials at the charm quark mass, which potentially account for all orders of $1/m_Q$ corrections. Furthermore, there is no restriction to dynamical calculation within this method.

In this paper, we present results of the spin-independent central and spin-spin potentials between the quark (Q) and antiquark (\bar{Q}) at the vicinity of the physical charm quark mass from the BS amplitude with 2+1 flavor PACS-CS gauge configurations [12], where the simulated pion mass is closest to the physical point as $M_\pi = 156(7)$ MeV. As for a treatment of heavy quarks, we adopt a relativistic heavy quark (RHQ) action, which can remove large discretization errors introduced by large quark mass [13].

TABLE I: Summary of RHQ parameters and results of S - and P -wave charmonium masses.

RHQ parameters	κ_c	ν	r_s	c_B	c_E		
	0.10819	1.2153	1.2131	2.0268	1.7911		
Charmonium mass	$M_{\text{ave}}^{S\text{-wave}}$	$M_{\text{hyp}}^{S\text{-wave}}$	$\eta_c (0^{-+})$	$J/\psi (1^{-+})$	$\chi_{c0} (0^{++})$	$\chi_{c1} (1^{++})$	$h_c (1^{+-})$
[GeV]	3.0638(9)	0.1124(9)	2.9794(5)	3.0919(10)	3.3865(58)	3.4781(62)	3.4995(62)

Let us briefly review the new method utilized here to calculate the interquark potential with the finite quark mass. As the first step, we consider the following equal-time $Q\bar{Q}$ BS amplitude in the Coulomb gauge for the quarkonium states [14, 15]:

$$\phi_\Gamma(\mathbf{r}) = \sum_{\mathbf{x}} \langle 0 | \bar{Q}(\mathbf{x}) \Gamma Q(\mathbf{x} + \mathbf{r}) | Q\bar{Q}; J^{PC} \rangle, \quad (1)$$

where \mathbf{r} is the relative coordinate of two quarks at certain time slice and Γ is any of the 16 Dirac γ matrices. A summation over spatial coordinates \mathbf{x} projects onto the zero total momentum. The \mathbf{r} -dependent amplitude, $\phi_\Gamma(\mathbf{r})$, is here called BS wave function.

In lattice simulations, the BS wave function can be extracted from the following four-point correlation function

$$\begin{aligned} & \sum_{\mathbf{x}, \mathbf{x}', \mathbf{y}'} \langle 0 | \bar{Q}(\mathbf{x}, t) \Gamma Q(\mathbf{x} + \mathbf{r}, t) (\bar{Q}(\mathbf{x}', t_s) \Gamma Q(\mathbf{y}', t_s))^\dagger | 0 \rangle \\ &= \sum_{\mathbf{x}} \sum_n A_n \langle 0 | \bar{Q}(\mathbf{x}) \Gamma Q(\mathbf{x} + \mathbf{r}) | n \rangle e^{-M_n^\Gamma(t-t_s)} \\ & \xrightarrow{t \gg t_s} A_0 \phi_\Gamma(\mathbf{r}) e^{-M_0^\Gamma(t-t_s)}, \end{aligned} \quad (2)$$

at the large Euclidean time from source location (t_s). Here both quark and antiquark fields at t_s are separately averaged in space as wall sources. The constant amplitude A_n is a matrix element defined as $A_n = \sum_{\mathbf{x}', \mathbf{y}'} \langle n | (\bar{Q}(\mathbf{x}') \Gamma Q(\mathbf{y}'))^\dagger | 0 \rangle$. M_n^Γ denotes a mass of the n -th quarkonium state $|n\rangle$ in a given J^{PC} channel. For instance, when Γ is chosen to be γ_5 for the pseudoscalar (PS) channel ($J^{PC} = 0^{-+}$) and γ_i for the vector (V) channel ($J^{PC} = 1^{-+}$) in the charm sector, M_0^{PS} and M_0^{V} correspond to the rest masses of the η_c and J/ψ ground states, which can be read off from the asymptotic large-time behavior of the correlation functions.

The BS wave function satisfies an effective Schrödinger equation with a nonlocal and energy-independent interquark potential U [11, 16]

$$-\frac{\nabla^2}{2\mu} \phi_\Gamma(\mathbf{r}) + \int dr' U(\mathbf{r}, \mathbf{r}') \phi_\Gamma(\mathbf{r}') = E_\Gamma \phi_\Gamma(\mathbf{r}), \quad (3)$$

where the reduced mass μ of the $Q\bar{Q}$ system is given by $m_Q/2$ with the quark kinetic mass m_Q . The energy eigenvalue E_Γ of the stationary Schrödinger equation is supposed to be $M_\Gamma - 2m_Q$ [17]. If the relative quark velocity $v = |\nabla/m_Q|$ is small as $v \ll 1$, the nonlocal potential U can generally expand in terms of the velocity v as

$U(\mathbf{r}', \mathbf{r}) = \{V(r) + V_S(r) \mathbf{S}_Q \cdot \mathbf{S}_{\bar{Q}} + V_T(r) S_{12} + V_{LS}(r) \mathbf{L} \cdot \mathbf{S} + \mathcal{O}(v^2)\} \delta(\mathbf{r}' - \mathbf{r})$, where $S_{12} = (\mathbf{S}_Q \cdot \hat{r})(\mathbf{S}_{\bar{Q}} \cdot \hat{r}) - \mathbf{S}_Q \cdot \mathbf{S}_{\bar{Q}}/3$ with $\hat{r} = \mathbf{r}/r$, $\mathbf{S} = \mathbf{S}_Q + \mathbf{S}_{\bar{Q}}$ and $\mathbf{L} = \mathbf{r} \times (-i\nabla)$ [11]. Here, V , V_S , V_T and V_{LS} represent the spin-independent central, spin-spin, tensor and spin-orbit potentials, respectively.

In this paper, we focus only on the S -wave charmonium states (η_c and J/ψ). We perform an appropriate projection with respect to the discrete rotation, which provides the BS wave function projected in the A_1^+ representation, $\phi_\Gamma(\mathbf{r}) \rightarrow \phi_\Gamma(A_1^+; r)$. This projected BS wave function corresponds to the S -wave in continuum theory at low energy [18]. We simply denote the A_1^+ projected BS wave function by $\phi_\Gamma(r)$ hereafter.

The stationary Schrödinger equation for the projected BS wave function $\phi_\Gamma(r)$ is reduced to

$$\left\{ -\frac{\nabla^2}{m_Q} + V(r) + \mathbf{S}_Q \cdot \mathbf{S}_{\bar{Q}} V_S(r) \right\} \phi_\Gamma(r) = E_\Gamma \phi_\Gamma(r) \quad (4)$$

at the leading order of the v -expansion [19]. The spin operator $\mathbf{S}_Q \cdot \mathbf{S}_{\bar{Q}}$ can be easily replaced by expectation values $-3/4$ and $1/4$ for the PS and V channels, respectively. As a result, both spin-independent and -dependent part of the central interquark potentials can be separately evaluated through a linear combination of Eq.(4) calculated for both PS and V channels as

$$V(r) = E_{\text{ave}} + \frac{1}{m_Q} \left\{ \frac{3}{4} \frac{\nabla^2 \phi_V(r)}{\phi_V(r)} + \frac{1}{4} \frac{\nabla^2 \phi_{\text{PS}}(r)}{\phi_{\text{PS}}(r)} \right\} \quad (5)$$

$$V_S(r) = E_{\text{hyp}} + \frac{1}{m_Q} \left\{ \frac{\nabla^2 \phi_V(r)}{\phi_V(r)} - \frac{\nabla^2 \phi_{\text{PS}}(r)}{\phi_{\text{PS}}(r)} \right\}, \quad (6)$$

where $E_{\text{ave}} = M_{\text{ave}} - 2m_Q$ and $E_{\text{hyp}} = M_V - M_{\text{PS}}$. The mass M_{ave} denotes the spin-averaged mass as $\frac{1}{4}M_{\text{PS}} + \frac{3}{4}M_V$. The derivative ∇^2 is defined by the discrete Laplacian with nearest-neighbor points. As for other spin-dependent potentials such as the tensor potential V_T and the spin-orbit potential V_{LS} , in principle, this approach can access them by considering the P -wave quarkonium states such as the χ_c (0^{++} , 1^{++}) and h_c (1^{+-}) states, which must leave contributions of V_T and V_{LS} to Eq.(4).

It is worth mentioning that the quark kinetic mass m_Q , which is essentially involved in the definition of the interquark potentials, can be self-consistently evaluated within the same framework [9]. The proper determination of the quark mass has a key role in establishing the connection to the static heavy-quark potential given by

Wilson loops in the infinitely heavy-quark limit. A more detailed discussion can be found in Ref. [9].

To calculate the charmonium potential, we have performed dynamical lattice QCD simulations on a lattice $L^3 \times T = 32^3 \times 64$ with 2+1 flavor PACS-CS gauge configurations generated by Iwasaki gauge action at $\beta = 1.90$, which corresponds to a lattice cutoff of $a^{-1} \approx 2.2$ GeV ($a \approx 0.091$ fm) [12]. The spatial lattice size corresponds to $L \approx 3$ fm. The hopping parameters for the light sea quarks $\{\kappa_{ud}, \kappa_s\} = \{0.13781, 0.13640\}$ correspond to $M_\pi = 156(7)$ MeV and $M_K = 554(2)$ MeV [12]. Although the light sea quark masses are slightly off the physical point, the systematic uncertainty due to this fact could be extremely small in our project. Our results are analyzed on all 198 gauge configurations, which are available through International Lattice Data Grid and Japan Lattice Data Grid [20]. We fix gauge configurations to Coulomb gauge.

For the charm quark, we employ the RHQ action to control systematic uncertainties coming from the discretization error induced by large quark mass [13]. The RHQ action utilized here is a variant of the Fermilab approach [21] and has five parameters κ_c, ν, r_s, c_B and c_E . The parameters r_s, c_B and c_E are determined by tadpole improved one-loop perturbation theory [22]. For ν , we use a nonperturbatively determined value, which is adjusted by reproducing the effective speed of light to be unity in the dispersion relation $E^2(\mathbf{p}^2) = M^2 + c_{\text{eff}}^2 |\mathbf{p}|^2$ for the spin-averaged $1S$ charmonium state, since the parameter ν is sensitive to the size of hyperfine mass splitting [23]. We choose κ_c to reproduce the experimental spin-averaged mass of $1S$ charmonium states $M_{\text{ave}}^{\text{exp}} = 3.0678(3)$ GeV. To calibrate adequate RHQ parameters, we employ a gauge invariant Gauss smearing source for the standard two-point correlation function with four different finite momenta. As a result, the relevant speed of light, $c_{\text{eff}}^2 = 1.04(5)$, is observed for the spin-averaged mass of $1S$ charmonium states with our chosen RHQ parameters summarized in Table I.

We have computed charm quark propagators with two wall sources located at different time slices $t_s/a = 6$ and 57 , to increase statistics. Dirichlet boundary conditions are imposed for the time direction to eliminate unwanted contributions across time boundaries. We calculate a pair of four-point correlation functions from two wall-source quark propagators and fold them together to create a single four-point correlation function.

Low-lying S - and P -wave charmonium masses measured in this study are all close to experimental values, though the hyperfine mass splitting $M_{\text{hyp}} = 0.1124(9)$ GeV is slightly smaller than the experimental value, $M_{\text{hyp}}^{\text{exp}} = 0.1166(12)$ GeV. Note that we simply neglect the disconnected diagrams in both the η_c and J/ψ correlation functions. The similar value of the hyperfine mass splitting is reported even on the physical point in Ref. [23]. We summarize resulting charmonium masses

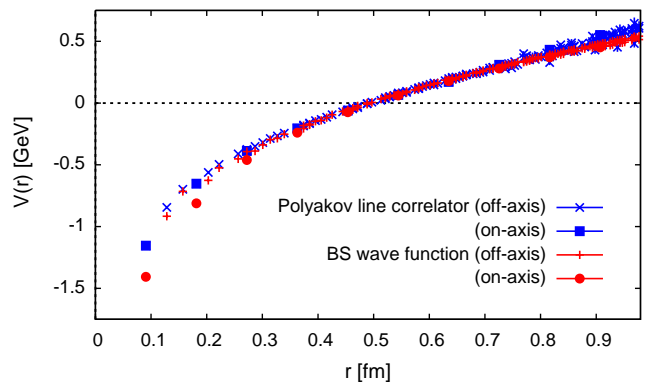


FIG. 1: Spin-independent interquark potentials calculated from both the BS wave function of the charmonium states (+ and ●) and the standard Polyakov line correlator (× and ■). Filled symbols represent on-axis data. The constant terms are subtracted from both potentials to set to $V(r_0) = 0$.

in Table I.

TABLE II: Summary of the Cornell parameters and the quark mass determined from lattice QCD. For comparison, the corresponding values adopted in a NRp model [5] are also included.

	This work		Polyakov lines	NRp model
	on-axis	full set		
A	0.861(17)	0.813(22)	0.403(24)	0.7281
$\sqrt{\sigma}$ [GeV]	0.394(7)	0.394(7)	0.462(4)	0.3775
m_Q [GeV]	1.74(3)		∞	1.4794

First, we show a result of the spin-independent charmonium potential $V(r)$ in Fig. 1, where the constant term is subtracted to set $V(r_0) = 0$ with the Sommer scale, $r_0 \approx 0.5$ fm. For comparison, the static heavy-quark potential calculated from the Polyakov line correlator, which corresponds to the one obtained in the infinitely heavy-quark limit similar to the Wilson loop results [6], is also displayed in Fig. 1. As expected, the charmonium potential calculated in the BS amplitude method properly exhibits the linearly rising potential at large distances and the Coulomb-like potential at short distances.

Here we give some technical remarks on systematic uncertainties. In the BS amplitude method, we take a weighted average of data points in the wide range of $|t - t_s|/a = 26 - 48$ for determining the equal-time BS wave function. Therefore, the resulting charmonium potential has a much smaller systematic error stemming from the uncertainty in the choice of time window than the conventional approach to calculate the static heavy-quark potential by Wilson-loops or Polyakov lines. On the other hand, the discretization error seems to much severely appear in the charmonium potential especially near the origin. The Coulomb-like behavior obtained in the BS amplitude method may contain large uncertain-

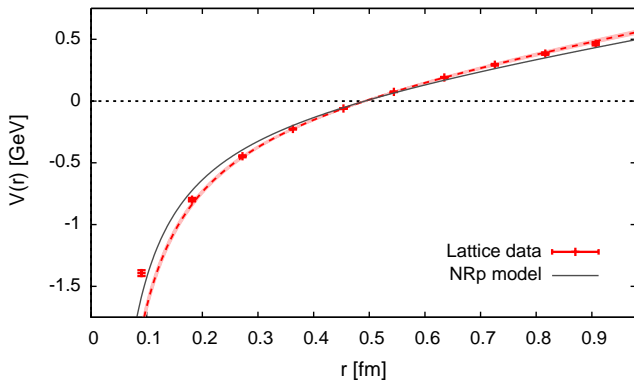


FIG. 2: Spin-independent charmonium potential calculated from the BS wave function. The dashed curve is the fitting result by the Cornell parametrization. The shaded band shows statistical fitting uncertainty calculated by the jack-knife method. For comparison, the phenomenological potential adopted in a NRp model [5] is also included as solid curve.

ties, which should vanish in the continuum limit. To avoid the large discretization error, we hereafter prefer to use the “on-axis” data, which less suffers from the rotational symmetry breaking in the finite cubic box.

The Cornell parametrization is simply adopted for fitting our data of the spin-independent central potential:

$$V(r) = -\frac{A}{r} + \sigma r + V_0 \quad (7)$$

with the Coulombic coefficient A , the string tension σ and a constant V_0 . We have carried out correlated χ^2 fits with full covariance matrix for on-axis data over range $4 \leq r/a \leq 10$, while uncorrelated fits are adopted in full data analysis including all off-axis data points due to high correlation between different r points. The fitting results are listed in Table I together with the phenomenological values employed by a nonrelativistic potential (NRp) model in Ref. [5]. From on-axis data only, we get the Cornell parameters of the charmonium potential: $A = 0.861(17)$ and $\sqrt{\sigma} = 0.394(7)$ MeV with acceptable χ^2/dof (≈ 2.2). The quoted errors represent only the statistical errors given by the jack-knife analysis.

In Fig. 2, we show on-axis data points of the spin-independent charmonium potential with the fitted curve (dashed curve). The phenomenological potential used in NRp models [5] is also plotted as a solid curve for comparison. As shown in Fig. 2, although the charmonium potential obtained from lattice QCD is quite similar to the one in the NRp models, the string tension of the charmonium potential is slightly stronger than the phenomenological one. Therefore our result indicates that there are only minor modifications required for the spin-independent central potential in the NRp models.

Moreover, it seems that a gap for the Coulombic coefficients between the conventional static potential from

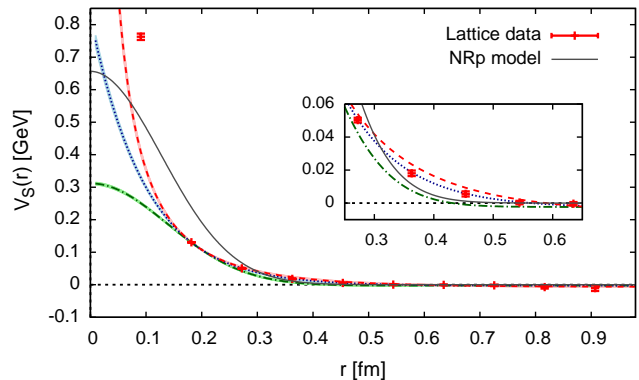


FIG. 3: Spin-spin charmonium potential calculated from the BS wave function. The dashed, dotted and dash-dotted curve correspond to fitting results of Yukawa, exponential and Gaussian functional forms, respectively. For comparison, the phenomenological potential adopted in a NRp model [5] is also included as solid curve.

Wilson-loops and the phenomenological potential used in the NRp models closes by our new approach, which non-perturbatively accounts for a finite quark mass effect.

It is worth mentioning that the string breaking, which would be induced by the presence of dynamical quarks was not observed at least in the range $r \lesssim 1$ fm, where we still get a better signal-to-noise ratio. It is indeed what we expected, since we cannot access information of the potential outside of the localized wave function, which represents the charmonium bound state within the BS amplitude method. We here calculate only the BS wave functions of $1S$ charmonium states, which are quickly dumped around outside of $r \gtrsim 1$ fm. Therefore, at least the similar calculation for the higher-lying charmonium states, whose wave function can be extended until the string breaking sets in, is demanded to observe such effect.

In this calculation, the kinetic mass of the charm quark is determined self-consistently within the BS amplitude method as well. (See Ref. [9] for details.) The charm quark mass obtained in this study is about 17% heavier than the one adopted in the NRp models, of which value is also listed in Table II. This difference should not be taken seriously since the spatial profile of the spin-spin potential from lattice QCD is slightly different from the one used in the NRp models as we will discuss later.

In Fig. 3, we show the spin-spin term of the charmonium potential and the corresponding phenomenological one found in Ref. [5]. Our spin-spin potential exhibits the short-range *repulsive interaction*, which is required by the charmonium spectroscopy, where the higher spin state in hyperfine multiplets receives heavier mass. It should be reminded that the Wilson loop approach fails to reproduce the correct behavior of the spin-spin interaction, since the leading-order spin-spin potential classified

TABLE III: Results of fitted parameters for the spin-spin potential with three types of the fitting functional form.

functional form	α	β	χ^2/dof
Yukawa-type	0.287(8)	0.894(32) GeV	7.28
Exponential-type	0.825(19) GeV	1.982(24) GeV	1.46
Gaussian-type	0.314(4) GeV	1.020(11) GeV ²	22.79

in potential nonrelativistic QCD becomes attractive at short distances [8].

In contrast of the case of the spin-independent potential, the spin-spin potential obtained here is absolutely different from a repulsive δ -function potential generated by perturbative one-gluon exchange, which is widely adopted in the NRp models. However, such the contact form $\propto \delta(\mathbf{r})$ of the Fermi-Breit type potential is not reliable since the pointlike spin-spin interaction can not give a finite hyperfine mass splitting of the P - or higher-wave charmonia [1]. Indeed, the finite-range spin-spin potential described by the Gaussian form is adopted in Ref. [5], where many properties of conventional charmonium states at higher masses are predicted.

This phenomenological spin-spin potential is also plotted in Fig. 3 for comparison. Although there is a slight difference at very short distances, where systematic uncertainties become severe due to lattice discretization errors, the spin-spin potential from first principles QCD is barely consistent with the phenomenological one.

To examine the appropriate functional form for the spin-spin potential, we have tried three types of functional forms:

$$V_S(r) = \begin{cases} \alpha \exp(-\beta r)/r & : \text{Yukawa form} \\ \alpha \exp(-\beta r) & : \text{Exponential form} \\ \alpha \exp(-\beta r^2) & : \text{Gaussian form.} \end{cases} \quad (8)$$

We then determine which functional form can give a reasonable fit over the range of r/a from 2 to 10. All results of correlated χ^2 fits are summarized in Table III. The long-range screening observed in the spin-spin potential is more easily accommodated by the Yukawa form or the exponential form than the Gaussian form that is often employed in the NRp models. Although the exponential form provides the smaller χ^2/dof than the Yukawa form, a solid conclusion requires more accurate information on the short-range behavior of the spin-spin potential.

In this paper, we have studied both spin-independent and spin-dependent part of the charmonium potential by means of the BS wave function of $1S$ charmonium states in dynamical lattice QCD simulations. The spin-independent charmonium potential obtained from lattice QCD with almost physical quark masses is quite similar to the one used in the NRp models. The spin-spin potential, which is, for the first time, determined in dynamical lattice simulations, exhibits not pointlike, but finite-range repulsive interaction. Its r -dependence is

barely consistent with the phenomenological one adopted in Ref. [5]. Thus, a full set of the reliable spin-dependent potentials derived from lattice QCD within our approach can provide new and valuable information to the NRp models. This improvement of the spin-dependent potentials will help in making accurate theoretical predictions about the higher-mass charmonium states. We plan to extend our research to determine all spin-dependent terms in the charmonium potential, including the tensor and spin-orbit forces and also to address all the possible systematic uncertainties described in the text.

We acknowledge the PACS-CS collaboration and ILDG/JLDG [20] for providing us with the gauge configurations. We would also like to thank H. Iida, Y. Ikeda and T. Hatsuda for fruitful discussions. This work was partially supported by JSPS/MEXT Grants-in-Aid (No. 22-7653, No. 19540265, No. 21105504 and No. 23540284).

* Electronic address: kawanai@nt.phys.s.u-tokyo.ac.jp

† Electronic address: ssasaki@phys.s.u-tokyo.ac.jp

- [1] M. B. Voloshin, Prog. Part. Nucl. Phys. **61**, 455 (2008).
- [2] S. Godfrey and S. L. Olsen, Ann. Rev. Nucl. Part. Sci. **58**, 51 (2008).
- [3] E. Eichten *et al.*, Phys. Rev. Lett. **36**, 500 (1976).
- [4] S. Godfrey and N. Isgur, Phys. Rev. D **32**, 189 (1985).
- [5] T. Barnes, S. Godfrey and E. S. Swanson, Phys. Rev. D **72**, 054026 (2005).
- [6] For a review, see G. S. Bali, Phys. Rept. **343**, 1 (2001).
- [7] N. Brambilla *et al.*, Rev. Mod. Phys. **77**, 1423 (2005).
- [8] Y. Koma and M. Koma, Nucl. Phys. B **769**, 79 (2007).
- [9] T. Kawanai and S. Sasaki, Phys. Rev. Lett. **107**, 091601 (2011).
- [10] Y. Ikeda and H. Iida, arXiv:1102.2097 [hep-lat].
- [11] N. Ishii, S. Aoki and T. Hatsuda, Phys. Rev. Lett. **99**, 022001 (2007), S. Aoki, T. Hatsuda and N. Ishii, Prog. Theor. Phys. **123** (2010) 89.
- [12] S. Aoki *et al.* [PACS-CS Collaboration], Phys. Rev. D **79**, 034503 (2009).
- [13] S. Aoki, Y. Kuramashi and S. I. Tominaga, Prog. Theor. Phys. **109**, 383 (2003).
- [14] B. Velikson and D. Weingarten, Nucl. Phys. B **249**, 433 (1985).
- [15] R. Gupta, D. Daniel and J. Grandy, Phys. Rev. D **48**, 3330 (1993).
- [16] W. E. Caswell and G. P. Lepage, Phys. Rev. A **18**, 810 (1978).
- [17] The relativistic effect has been estimated using relativistic kinematics in Ref. [10]. Although the short-range behavior of interquark potential is slightly influenced by this modification, it is indeed small for the heavier quarks such as the charm quark.
- [18] M. Lüscher, Nucl. Phys. B **354**, 531 (1991).
- [19] Here, we essentially follow the NRp models, where the J/ψ state is purely composed of the $1S$ wave function. However, within this method, this assumption can be verified by evaluating the size of a mixing between $1S$ and $1D$ wave functions in principle.
- [20] International Lattice Data Grid/Japan Lattice Data

Grid, <http://www.jldg.org>.

- [21] A. X. El-Khadra, A. S. Kronfeld and P. B. Mackenzie, *Phys. Rev. D* **55**, 3933 (1997).
- [22] Y. Kayaba *et al.* [CP-PACS Collaboration], *JHEP* **0702**, 019 (2007).
- [23] Y. Namekawa *et al.* [PACS-CS Collaboration], arXiv:1104.4600 [hep-lat].